MOLECULAR
METABOLISM

Nicotinamide riboside alleviates exercise intolerance in ANT1-deficient mice

Patrick M. Schaefer [1], Jessica Huang [1], Arrienne Butic [1], Caroline Perry [2], Tal Yardeni [1], Wendy Tan [1],
Ryan Morrow [1], Joseph A. Baur [2], Douglas C. Wallace [1,3],*

ABSTRACT

Objective: Mitochondrial disorders are often characterized by muscle weakness and fatigue. Null mutations in the heart-muscle adenine nucleotide translocator isoform 1 (ANT1) of both humans and mice cause cardiomyopathy and myopathy associated with exercise intolerance and muscle weakness. Here we decipher the molecular underpinnings of ANT1-deficiency-mediated exercise intolerance.
Methods: This was achieved by correlating exercise physiology, mitochondrial function and metabolomics of mice deficient in ANT1 and comparing this to control mice.
Results: We demonstrate a peripheral limitation of skeletal muscle mitochondrial respiration and a reduced complex I respiration in ANT1-deficient mice. Upon exercise, this results in a lack of NAD^+ leading to a substrate limitation and stalling of the TCA cycle and mitochondrial respiration, further limiting skeletal muscle mitochondrial respiration. Treatment of ANT1-deficient mice with nicotinamide riboside increased NAD^+ levels in skeletal muscle and liver, which increased the exercise capacity and the mitochondrial respiration.
Conclusion: Increasing NAD^+ levels with nicotinamide riboside can alleviate the exercise intolerance associated to ANT1-deficiency, indicating the therapeutic potential of NAD^+-stimulating compounds in mitochondrial myopathies.

1. INTRODUCTION

Adenine nucleotide translocators (ANTs) mediate ADP/ATP exchange across the inner mitochondrial membrane exchanging ATP from the mitochondrial matrix with ADP from the cytosol. In addition, the ANTs are essential role in mitophagy, provide a voltage sensitive proton channel and regulate the mitochondrial permeability transition pore (mPTP) [1—4].

There are three isoforms of ANTs in humans, which show a tissue-specific expression pattern. Null mutations in the nuclear-encoded heart/muscle isoform ANT1 cause mitochondrial myopathy and cardiomyopathy in humans [5,6]. Certain missense mutations in the human ANT1 gene can manifest as autosomal dominant progressive external ophthalmoplegia [7]. ANT1-null patients show elevated serum lactate levels, decreased phosphocreatine levels in muscle and exercise intolerance consistent with an impaired ATP export from the mitochondria. In addition, patients show ragged red muscle fibers and accumulation of aberrant mitochondria due to the defect in mitophagy [5,6].

Mice deficient for ANT1 ($Slc25a4^{-/-}$) manifest a severe exercise intolerance, cardiomyopathy, ragged red muscle fibers, mitochondrial hyperproliferation, impaired coupled respiration, and increased uncoupling of skeletal muscle mitochondria [8,9]. In addition, glucose homeostasis is altered in ANT1-deficient mice, demonstrating an improved insulin-sensitivity, glucose tolerance and resistance to high-fat diet [10,11]. In summary, the ANT1-deficient mouse model mirrors the human pathology with respect to myopathy, cardiomyopathy and exercise intolerance [9]. Thus, exercise intolerance in ANT1-deficient mice could serve as a marker for muscle dysfunction in humans.

It is known that NAD^+ levels decrease with age and are lowered in many disorders with an underlying mitochondrial dysfunction [12,13]. Boosting NAD^+ levels with compounds such as nicotinamide riboside (NR) or nicotinamide mononucleotide (NMN) can be beneficial in a range of metabolic disorders (reviewed in [14]), including neurodegeneration [15], obesity [16] and diabetes [17]. Similarly, NAD^+-boosting compounds have been shown to rescue exercise intolerance and mitochondrial myopathy in mouse models of mitochondrial disease and in patients with adult-onset mitochondrial myopathy [18—20]. In the current study we delineate the physiological limitations underlying the exercise intolerance in ANT1-deficient mice. We then show that nicotinamide riboside can alleviate the associated exercise intolerance.

[1]Center for Mitochondrial and Epigenomic Medicine, Division of Human Genetics, Department of Pediatrics, Children's Hospital of Philadelphia, PA, 19104, USA [2]Department of Physiology and Institute for Diabetes, Obesity, and Metabolism, Perelman School of Medicine, University of Pennsylvania, Philadelphia, PA, USA [3]Department of Pediatrics, Perelman School of Medicine, University of Pennsylvania, Philadelphia, PA, 19104, USA

*Corresponding author. 3501 Civic Center Blvd, CTRB 6060, Philadelphia, PA, 19104, USA. E-mail: wallaced1@chop.edu (D.C. Wallace).

Brief Communication

2. MATERIAL AND METHODS

2.1. Mouse strains
All mouse strains used for this study are on the C57BL/6[Eij] (Nnt^{+/+}) background, which served as "B6 control" mice. ANT1 mice are deficient for the nuclear-encoded adenine nucleotide translocator 1 (ANT1, Slc25a4^{−/−}). In addition, they harbor the complex I subunit variant ND5 m.12352C>T (ND5[S204F]). To differentiate between the effect of the ANT1 mutation and a possible effect of the ND5 variant, we created mice harboring only the mtDNA variant ND5 m.12352C>T (ND5[S204F]) (ND5 mice) as additional controls.

Mice were fed 5LOD diet (irradiated 5001 standard low-fat diet for mice housed in barrier facility) from PicoLab and kept on a 12:12 h light—dark cycle. The Institutional Animal Care and Use Committee from the Children's Hospital of Philadelphia approved all protocols, and the protocols comply with all relevant ethical regulations regarding animal research.

2.2. NR treatment
Nicotinamide riboside chloride (NR) powder was received from ChromaDex and stored light protected at 4 °C. The average food consumption of mice was estimated at 3 g food/24 h for a 30 g mouse following previous measurements in a comprehensive lab animal monitoring system. We prepared the NR diet targeting a daily dose of 400 mg NR/kg body weight by mixing NR with powdered 5LOD (1:250) and water and forming pellets of 5—10 g, which were air-dried for 48 h under a flow hood in the dark and subsequently stored light protected at 4 °C for a maximum of 7 days. Fresh NR diet pellets were provided daily (5 g/mouse, 6 g for ANT1 mice) and old, remaining food was removed. Food consumption was recorded for each cage containing 1—5 mice. Average food consumption is displayed in Figure 4i with control-diet mice eating 3.72 g (B6 control) and 3.89 g (ANT1) per day.

2.3. Metabolic treadmill
Mice were acclimatized for 15min on the treadmill with the belt un not moving und the incline at 0°. For the exercise stress test, a stepwise ramp protocol was used. The first step at 3 m/min was held for 5min Subsequently, the speed was increased every 2min to 5/7.5/10 m/min continuing in steps of 2 m/min. At 12/16/20/26/30 m/min the speed was maintained for 4min with the incline being increased to 5/10/15/20/25° after 2min of the respective interval. Exhaustion was defined as 5 consecutive seconds on the shock grid (0.35 mA, 1shock/sec). The belt was stopped, the shock grid turned off and mice were kept in the treadmill for another 12min for recording of the recovery period. VO_2/VCO_2 during running at a sampling rate of 12/min with an airflow of 0.5 L/min using an Oxymax (Columbus Instruments) that was calibrated once per day using a mix of 20.5% O_2 and 0.5% CO_2.

For hyperoxia running, the air intake was connected to an oxygen tank containing 100% oxygen. Oxygen values for were out of range for the Oxymax but VCO_2 and running time was quantified.

2.4. Comprehensive lab animal monitoring system (CLAMS)
The Comprehensive Lab Animal Monitoring System was enclosed by an environmental chamber (Columbus Instruments) and combined with an 8-channel Oxymax system (Columbus Instruments). The system was calibrated once every 2 days using a mix of 20.5% O_2 and 0.5% CO_2. Air flow was set to 0.5 L/min per cage.

Mice were weighted and put in the CLAMS (Columbus Instrument) during the morning (10am to noon). Mice were kept at 23 °C and a 12:12 light dark cycle. Every 15min VO_2, VCO_2, activity, running wheel activity and food consumption were quantified starting the following day at 7am for a duration of 24 h. RER (VCO_2/VO_2) and energy expenditure (heat=(3.815 + 1.232*RER)*VO_2) were calculated from the data.

For the cold exposure, CLAMS were cooled down to 4 °C for 4 h, ending cold exposure with beginning of the light cycle at 7am.

2.5. Rotarod
18-month-old mice were acclimatized to the rotarod prior to the first session by sitting on the non-moving rod for 1min and subsequently walking on the rod at the slowest speed (5rpm) for 1min. If mice fell, they were placed back on the rod during the acclimatization. Mice were tested for 3 consecutive days with 3 trials each day with 30min intertrial rest in their home cage. For the trials, the rod was accelerating linearly from 5rpm to 40rpm within 4min and stayed at 40rpm until the maximal test period of 10min. Time until fall was quantified, with 2 consecutive loops without intermitted walking movement equals a fall). The average across all 9 trials was calculated.

2.6. Grip strength
18-month-old mice were grabbed by the base of their tail and allowed to hold on to a horizontal metal bar connected to a dynamometer with their front paws. They were slowly pulled away perpendicularly from the metal bar until they could not hold on anymore and the corresponding strength (N) was quantified. This was repeated consecutive 3 times in 1 session for a total of 3 sessions with 30min recovery in their home cage in between. The average grip strength across all 9 trials was calculated for each mouse.

2.7. Lactate measurements and blood gas analysis
Immediately after exhaustive exercise (Exer 3/6 treadmill, 2 m/min continuous acceleration at 10% incline for B6 control mice and 5% incline for ANT1 mice) or after sitting on the non-moving treadmill for 5min, blood was drawn using submandibular bleeding. Lactate measurements were performed using Lactate Plus Meter Test Strips (Nova biomedical). Blood gas analysis was performed using i-STAT CG8+ cartridges.

2.8. Muscle pO_2 measurements
Mice were anesthetized using 3% isoflurane in 100% oxygen and were placed on a heat pad to maintain body temperature. The gastrocnemius muscle and the sciatic nerve were uncovered and an oxygen/temperature bare fiber sensor (NX-BF/OT/E, connected to an OxyLite Pro XL) was inserted into the muscle. The sensor was minimally adjusted until a stable pO_2 plateau was reached. Subsequently the sciatic nerve was stimulated three times using a nerve stimulator (Grass SD9 Stimulator, 5 V, 10 ms pulses). The first stimulation was at 10 Hz for 30sec, the 2nd was at 5 Hz for 1min, and the 3rd was at 2.5 Hz for 2min, with at least 4min recovery period between stimulations or until pO_2 plateau was reached. The pO_2 was continuously recorded using LabChart and the pO_2 levels before/after stimulation as well as the average and maximal slope in the decreasing muscle pO_2 during stimulation were quantified. Results for each stimulation frequency were normalized to control and subsequently combined.

2.9. Fluo-respirometry
Mitochondrial respiration and reactive oxygen species (ROS) production in soleus muscle were assessed using the Oroboros Oxygraph-2K FluoRespirometer (Oroboros Instruments) as described previously [21]. Air calibration was performed in Mir05Cr respiratory buffer [0.5 mM EGTA, 3 mM MgCl2, 60 mM lactobionic acid, 20 mM taurine, 10 mM KH2PO4, 20 mM HEPES, 110 mM D-sucrose, and fatty acid-free BSA

(1 g/L) with the addition of 20 mM creatine and 5 mM DTPA] using the following settings: oxygen sensor gain: 2, gain of fluorescence-module-green: 300, data recording interval: 2 s, block temperature: 37 °C, stirrer speed: 750rpm. For ROS measurements 2 μl of 10 mM Amplex™ UltraRed (Thermo Fisher Scientific), 2 μl of peroxidase (500 U/ml → 0.5U/ml final concentration), 2 μl of superoxide dismutase (5 U/ml → 5mU/ml) were added to each chamber. ROS calibration was performed for each run by adding 2×4 μl of 100 μM hydrogen peroxide (2×0.2 μM). Using this approach, both superoxide anion as well as hydrogen peroxide production under different respiratory states can be quantified.

Soleus muscle was dissected from mice and cut perpendicularly starting at the distal end. This mechanical permeabilization protocol used here instead of a more traditional saponin-permeabilization allowed to reduce the time from sacrificing the mice to respirometry measurements and shows a comparable permeabilization efficiency [22]. Two muscle pieces were weighed, suspended in Mir05Cr respiratory buffer and added into a respiration chamber in 400 μl of Mir05Cr (performed in technical duplicates).

Subsequent addition of substrates allowed assessment of different respiratory states. First, 5 μl of 2 M pyruvate (2.5 mM), 2.5 μl of 400 mM malate (0.5 mM), and 10 μl of 2 M glutamate (10 mM) (PMG) were added, followed by 20 μl of 0.5 M adenosine diphosphate (5 mM) to provide complex I respiration. Addition of 20 μl of 1 M succinate (10 mM) results in OxPhos capacity. 0.5 μl of 10 mM oligomycin (2.5 μM) blocked complex V and provides Leak respiration, followed by titration of the uncoupler carbonyl cyanide-p-trifluoromethoxyphenylhydrazone (FCCP, 1 mM stock in 1 μl increments (~1.5 μM)) to reveal the electron transport system capacity (ETS capacity). 5 μl of 1 mM rotenone (2.5 μM) was added, resulting in complex II respiration. Finally, 2 μl of 5 mM antimycin A (5 μM) blocked CIII, providing non-mitochondrial background respiration, which was subtracted from all other respiratory states. CI capacity was calculated as the higher value of: (coupled respiration with PMG) or (ETS capacity minus respiration after rotenone). Likewise CII capacity is the higher value of: (OxPhos capacity minus coupled PMG) or uncoupled respiration after rotenone. Both approaches for CI capacity are suboptimal since "coupled respiration with PMG" could be limited by complex V and "ETS minus rotenone" could be limited if CI + CII capacity > CIII or CIV capacity. However, addition of succinate in the coupled state does further increase respiration significantly, suggesting that coupled respiration upon complex I substrates does provide a correct value for complex I capacity in our measurements.

Reoxygenation of the chambers at the end of the titration protocol allowed a quantification of ROS production at the same respiratory state with 2 different oxygen concentrations. The resulting equation was used to correct ROS production for the effect of O2 concentration in the chamber [22]. In addition, ROS production in the presence of all uncouplers and inhibitors provides a surrogate marker for mitochondrial mass [22]. Data were recorded and analyzed using DatLab7.

2.10. Fluorescence lifetime imaging microscopy (FLIM) of NAD(P)H

Immediately after cervical dislocation of a mouse, one gastrocnemius muscle was dissected and placed in Tyrodes buffer. A muscle bundle was separated carefully in Tyrodes buffer and placed on an LSM710 (Zeiss) in an imaging chamber (Warner Instruments) in Tyrodes buffer. Imaging was performed at room temperature within 30min of preparation using a 20x lense (NA: 0.8) and pulsed, 2-photon excitation (730 nm, 80 MHz, 10fs pulse width, 5 mW poweder on sample, 1min excitation time) of NAD(P)H. NAD(P)H autofluorescence lifetime was detected through a 460/50 nm bandpass filter using time-correlated single photon counting (HPM-100-40, Becker&Hickl) with a time resolution of 256 time channels within the 12.5ns pulse period (512x512 pixels, 15μsec pixel dwell time, SPCM 9.8). A biexponential decay with lifetime components fixed to 400ps (free NAD(P)H) and 2500ps (protein-bound NAD(P)H) was fitted to the NADH autofluorescence decay curve for every pixel (bin 2) using SPCImage 8.0 and the mean NAD(P)H lifetime (τ_{mean}) was quantified for every image.

2.11. Global metabolomics

After exhaustive exercise (Exer 3/6 treadmill, 1 m/min continuous acceleration at 10% incline for B6 control mice and 5% incline for ANT1 mice) or after sitting on the non-moving treadmill for 5min mice were cervically dislocated and the gastrocnemius muscle was dissected first and immediately flash frozen in liquid nitrogen and stored at −80 °C.

2.12. Untargeted LC/MS metabolomics

Wet, frozen mouse gastrocnemius samples were lyophilized overnight and powdered in a Precellys homogenizer (Bertin Technologies) at 4 °C. Approximately 5 mg aliquots of dry tissue powder were homogenized in 500 μl of 80% ice cold methanol in the Precellys homogenizer at 4 °C. Then, 100 μl of homogenates were extracted with 400 μl of ice-cold methanol, vortexed, centrifuged at $18,000 \times g$, and 400 μl aliquots of supernatants were dried under nitrogen at 45 °C in a 96-well plate. Samples were reconstituted in 10% methanol for reversed-phase C18 chromatography or 50% methanol for HILIC chromatography with gradient elution. In addition, 10 μl of each homogenate was pooled together, divided into 100 μl aliquots, and extracted according to the above protocol to make QC samples. Samples were analyzed by a Thermo Vanquish UHPLC/Orbitrap ID-X mass spectrometer scanned from m/z 60−1000 at a resolution of 120,000. Compound Discoverer (Thermo Fisher Scientific) was used to generate PCA plots from the metabolite signals extracted from the raw data files, fold changes, p-values, heat maps, whisker plots, and perform a database search for metabolite identification. Pathway analysis for global metabolomics were performed using significantly up or downregulated metabolites (nominal p-value < 0.05) in Metascape [23]. The raw data were unloaded on Metabolights and can be accessed via: https://www.ebi.ac.uk/metabolights/MTBLS4312/descriptors. Click or tap if you trust this link.">https://www.ebi.ac.uk/metabolights/MTBLS4312/descriptors

2.13. Targeted LC/MS metabolomics

Approximately 5 mg aliquots of dry gastrocnemius powder were homogenized in 500 μl of 50% acetonitrile/0.3% formic acid for the extraction of organic acids and malonyl and acetyl CoA. Additional 5 mg aliquots of dry tissue powder were homogenized in 500 μl of 80% methanol for the extraction of nucleotides in a similar way to the untargeted metabolomics protocol above. Aliquots (100 μl) of the homogenates prepared for organic acids and malonyl and acetyl CoA were extracted and quantitated by LC/MS according to validated, optimized protocols in our previously published studies [24,25]. Nucleotides were extracted from 100 μl homogenates with 400 μl of ice-cold methanol and processed further according to the untargeted metabolomics protocol above prior to LC/MS. An Agilent PEEK poroshell HILIC-z column was used to separate nucleotides with gradient elution. Quantitation of metabolites in each assay module was achieved using multiple reaction monitoring of calibration solutions and study samples on an Agilent 1290 Infinity UHPLC/6495 triple quadrupole mass spectrometer. Raw data were processed using Mass Hunter quantitative analysis software (Agilent). Calibration curves

Brief Communication

(R2 = 0.99 or greater) were either fitted with a linear or a quadratic curve with a $1/X$ or $1/X^2$ weighting.

2.14. NAD/NADH quantification

For quantification of NAD and NADH in gastrocnemius muscle, we powdered flash frozen gastrocnemius on dry ice, split the powder into 4 tubes, quantified the weight, flash froze the gastrocnemius powder in liquid nitrogen and stored at $-80\ ^{\circ}C$.

Two tubes were used for the NAD/NADH cycling assay. For NAD, powdered tissue was lysed in ice-cold 0.6 M Perchloric Acid, for NADH in ice-cold 0.25 M KOH in 50% ethanol and spun down for 15min at 20,000 g at 4 $^{\circ}$C. Supernatant is transferred to a new tube and diluted 1:40 (1:25 for NADH) in ice cold Na-Phosphate buffer (pH 8.0). NAD standards or diluted extracts were added to a cycling mixture consisting of 2% ethanol, 100 μg/mL alcohol dehydrogenase, 10 μg/mL diaphorase, 20 μM resazurin, 10 μM flavin mononucleotide, 10 mM nicotinamide, 0.1% BSA in 100 mM phosphate buffer, pH 8.0. Fluorescence was quantified at 590 nm (ex:530 nm) in a 96 well plate.

One tube was used for NAD/NADH quantification using the NAD/NADH-Glo™ Assay (Promega) following the manufacturer's protocol. In short, the gastric powder was lysed in 1% DTAB (Sigma Cat.#D8638) in 0.2 N NaOH. Subsequently, samples were split and heated to 60 $^{\circ}$C for 15min in the base solution (for NADH measurements) or after addition of 1:2 volumes of 0.4 N HCl (for NAD + measurements). After buffering of the samples with HCL/Trizma solution (0.4 N HCl+0.5 M Trizma base) or Trizma base (12.1 g Trizma base in 200 mL water), the NAD/NADH-Glo™ Assay was performed. The results of both assays were normalized to the average across all samples and subsequently combined for each mouse.

For quantification of NAD(H) levels in isolated mitochondria from gastrocnemius muscle, the muscle was minced in PBS supplemented with 10 mM EDTA and 0.05% trypsin on ice for 20 min. It was further homogenized in H buffer (225 mM mannitol, 75 mM sucrose, 10 mM Mops, 1 mM EGTA, 0.2% BSA, pH 7.4) using a dounce homogenizer with the pestle rotation speed of 1100 rpm for $10-20$ strokes. The homogenate was spun down at 800 g for 5 min, and then washed and spun down one additional time. The supernatant was removed and spun at 8000 g to pellet the mitochondria. The pellets were resuspended in 100 μl of 1% DTAB (Sigma Cat.#D8638) in 0.2 N NaOH. They were buffered using HCL/Trizma solution (0.4 N HCl+0.5 M Trizma base), the NAD(H) was quantified using the NAD/NADH-Glo Glo™ Assay (Promega) and normalized to mitochondrial protein amount.

2.15. Statistics

For all data that were performed in technical replicates (Oroboros [2], muscle pO$_2$ [3], NAD(H) quantification $[2-6]$, NAD(P)H FLIM [5]), the mean of all replicates was calculated and used as one independent datapoint. All data points displayed in the graphs are independent and statistical tests were performed on independent samples. The only limitation to the independence of mice was that all mice within a cage had to undergo the same treatment (NR or untreated) since we wanted to avoid extended single-housing and the treatment was administered with the food. Gaussian distribution of the data was checked using a D'Agostino & Pearson omnibus normality test (significance level $\alpha < 0.05$). If the normality test was passed an unpaired two-tailed t-test was performed, if the normality test failed a Mann—Whitney test was used.

The effects of NR in tests that were performed before and after NR diet (metabolic treadmill) are displayed as fold change normalized to untreated mice and calculated as:

$$\left(NR_{post} / NR_{prior} \right) / \left(untreated_{post} / untreated_{prior} \right)$$

This normalization was performed to correct for potential changes in the parameters with age in the untreated cohort. The effects of NR in tests that were performed only after NR diet (CLAMS, Oroboros, NAD(P)H FLIM, metabolites) are displayed as fold change normalized to untreated mice and calculated as:

$$NR_{post} / untreated_{post}$$

Significances between strains were indicated graphically as (*) and between acutely exercised and rested or between NR-fed or control diet as (#) (*/#p < 0.05, **/##p < 0.01, ***/###p < 0.001). Statistics for global metabolomics are described in the respective methods section.

3. RESULTS

3.1. VO$_2$ is decreased in ANT1 mice during exercise, contributing to their exercise intolerance

We assessed the exercise capacity in C57Bl/6 mice (control) and $Slc25a4^{-/-}$ ($ANT1^{-/-}$) mice ranging from 24 weeks until 70 weeks of age. As observed previously, ANT1 mice show a lower VO$_{2max}$ and a shorter time until exhaustion in the ramp test on a metabolic treadmill already by 6 months of age (Figure 1A). By contrast, ANT1 mice reach their VO$_{2max}$ shortly after the start of the exercise stress test and subsequently their VO$_2$ declines despite an increasing exercise intensity (Figure 1A, blue line). In control mice, VO$_2$ steadily increases with exercise intensity, reaching VO$_{2max}$ upon exhaustion (Figure 1A, black line).

Looking at the RER trace during the exercise stress test, control mice show a relatively steady RER of 0.8 for the first two thirds of the exercise stress test and a subsequent increase, indicating an increased carbohydrate usage upon high exercise intensity (Figure 1B). In contrast, the RER increases very fast in ANT1 mice starting at the time point of VO$_{2max}$ (Figure 1B). This demonstrates that reduced oxygen uptake coincides with a fast switch from fat to predominantly carbohydrate fuel usage in ANT1 mice, likely due to increased glycolytic energy production. As expected, VO$_{2max}$ and running time (time until exhaustion in the exercise stress test ramp protocol) decrease with age in B6 control mice (Figure 1C), as does running time in ANT1 mice (Figure 1D). However, VO$_{2max}$ does not decrease in ANT1 mice with age, but the VO$_2$ decrease upon running becomes more exaggerated, demonstrated by calculating a ratio of the VO$_2$ at exhaustion (VO$_{2end}$) and the VO$_{2max}$. Thus, in ANT1 mice VO$_{2end}$/VO$_{2max}$ correlates with the running performance over age (Figure 1D), suggesting that decreasing VO$_2$ during exercise is an important factor in the exercise intolerance of ANT1 mice.

To further understand the decreasing VO$_2$ during endurance exercise in ANT1 mice, we first tested for a psychological or motor limitation, preventing the ANT1 mice to exhaust themselves physically in the exercise stress test. Maximal RER is used as a measure of exhaustion with RER >1.0 indicating exhaustion [26]. Both ANT1 as well as control mice show an average RER$_{max}$ of >1.0, with ANT1 mice rather reaching a non-significantly higher RER$_{max}$ compared to control (Figure 1E). In addition, in ANT1 mice both RER and VO$_2$ show a longer recovery period to baseline after an exercise stress test (Figure 1a and b).

We measured blood lactate levels both at rest and immediately after an exercise stress test. ANT1 mice showed higher lactate levels at rest and after exercise compared to B6 control mice, resulting in a similar
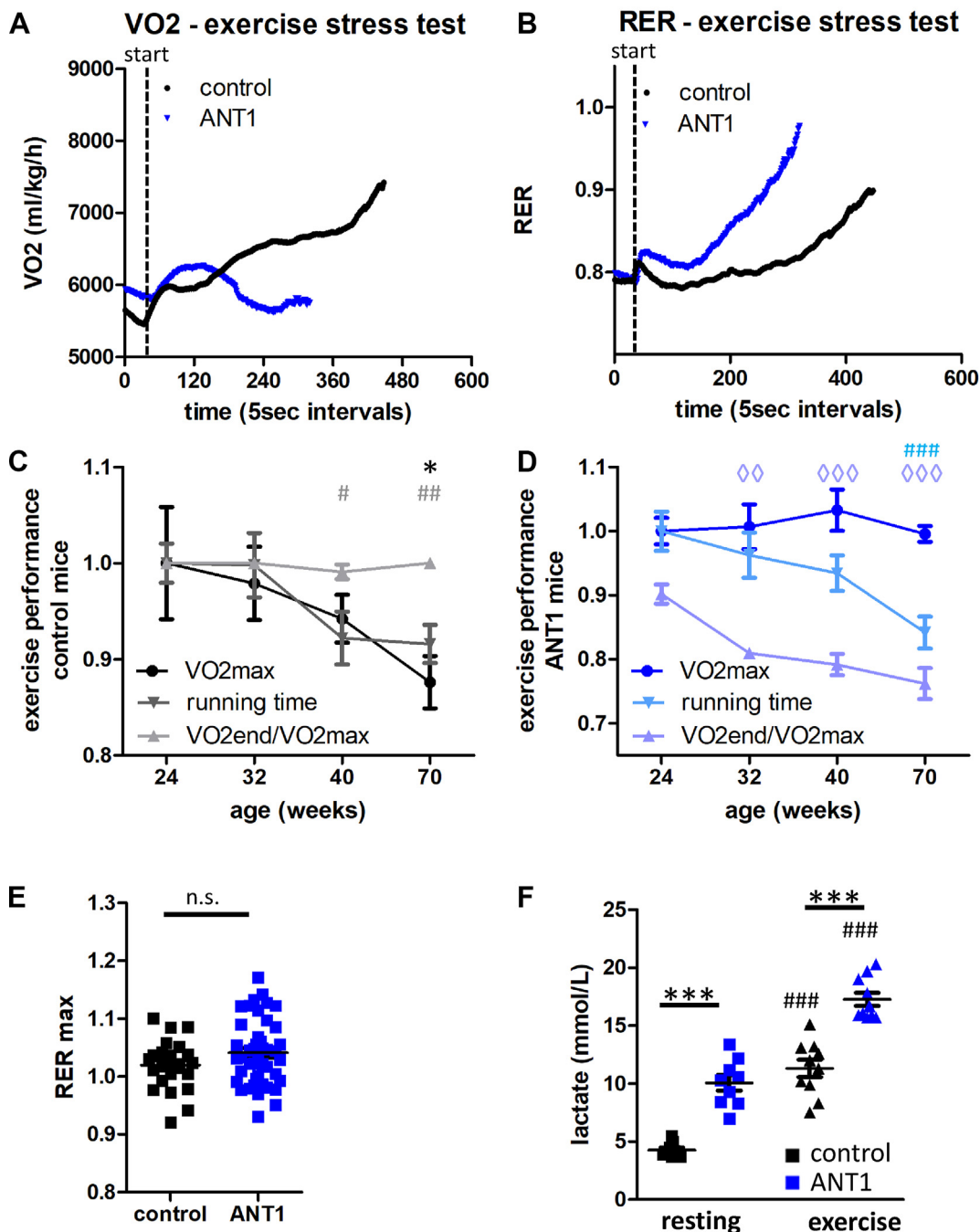
Figure 1: VO$_2$ decreases in ANT1 mice during exercise. **A/B)** Kinetics of the average oxygen uptake (VO$_2$) (A) and respiratory exchange ratio (RER, VO$_2$/VCO$_2$) (B) of 4-month-old mice during an exercise stress test (ramp protocol) on a metabolic treadmill (n = 24−40, curve displayed until >50% of the animals quit). **C/D)** Display of exercise performance parameters (VO$_2$max, running time, VO$_2$end/VO$_2$max) in B6 control mice (C) and ANT1 mice (D) over age normalized to performance at 24 weeks (n = 7−9, error bars indicate SEM). Significances were calculated compared to performance at 24 weeks of age and are indicates as * for VO$_2$max, # for running time and ◇ for VO$_2$endVO$_2$max. **E)** Maximal RER reached during the exercise stress test (n = 24−40). **F)** Blood lactate levels in resting mice and immediately after exhaustive exercise (n = 9−10, 6-9-month-old). Significances between strains (*) and between "exercise" and "resting" (#) were calculated using Mann Whitney test (*p < 0.05, **p < 0.01, ***p < 0.0001).

increase in blood lactate levels upon exercise (Figure 1F). Thus, ANT1 mice show to higher tolerance of exhaustion compared to B6 control mice. Furthermore, we tested motor coordination in 18-month-old ANT1 and control mice and found a similar performance on the rotarod (Figure S1c), indicating no motor phenotype that could explain a reduced exercise performance on the treadmill. Similarly, grip strength was not reduced in 18-month-old ANT1 mice compared to control

(Figure S1d), suggesting no deficit in muscle strength. In summary, we demonstrated a reduced exercise capacity in ANT1 mice due to physical limitation.

3.2. Skeletal muscle oxygen consumption limits VO$_2$ in ANT1 mice
Physical factors limiting VO$_{2max}$ can be divided into a central limitation by the cardiovascular system and the transport of oxygen to the
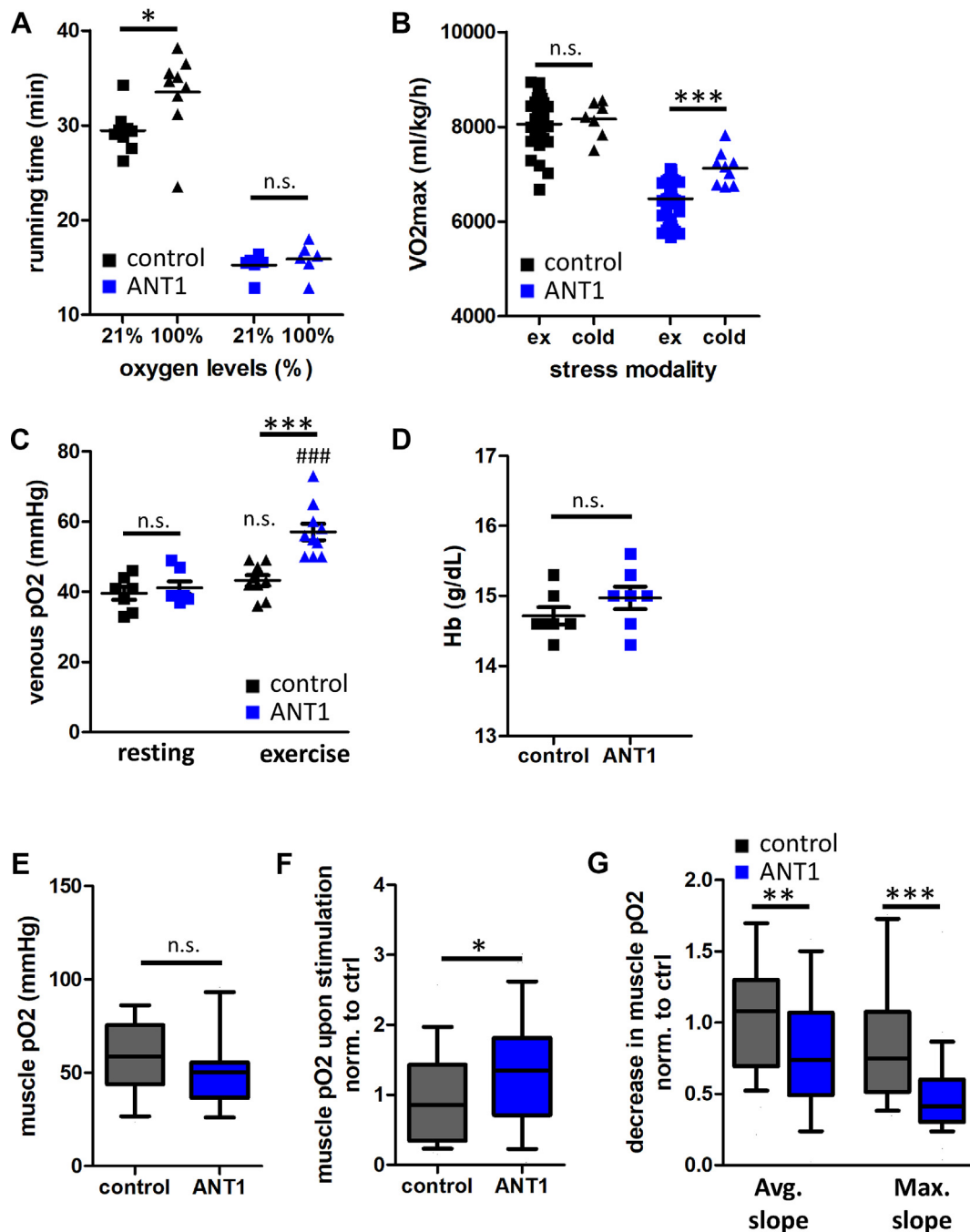
Figure 2: Skeletal muscle oxygen consumption limits VO₂ in ANT1 mice. **A)** Time until exhaustion in an exercise stress test (ramp protocol) performed at normoxia (21% oxygen) or hyperoxia (100% oxygen) in the same mice (n = 6–9). Significances between normoxia and hyperoxia were calculated using Wilcoxon signed rank test. **B)** VO₂max reached in an exercise stress test (ex, n = 39–44) or during a 4 h cold exposure (cold, n = 7–9, 4 °C) in 4-month-old mice. Significances between stress modalities were calculated using unpaired t-test. **C)** pO₂ in blood from the submandibular vein in resting mice and immediately after exhaustive exercise (n = 7–10, 6-9-month-old). Significances between strains (*) and between "exercise" and "resting" (#) were calculated using Mann Whitney test. **D)** Hemoglobin levels in blood from the submandibular vein in resting mice (n = 7, 6-9-month-old). **E/F/G)** Muscle pO₂ in non-stimulated M. gastrocnemius of anesthetized mice (6-12-month-old) (E). Muscle pO₂ (F) and rate of decay in muscle pO₂ (G) upon sciatic nerve stimulation normalized to B6 controls (n = 17–18, 3 technical replicates). Whisker plots show 10–90% intervals, significances between strains were calculated using Mann−Whitney test.

muscles or peripheral limitation by the mitochondrial oxygen consumption of the muscles. We assessed whether ANT1 mice are centrally or peripherally limited in their VO₂.

First, we performed an exercise stress test at 100% oxygen, thereby increasing oxygen availability. This resulted in an increase in running time in B6 control mice but no change in ANT1 mice compared to running under normoxia. This shows a central limitation in control mice but a peripheral limitation in ANT1 mice (Figure 2A). Next, we compared VO₂max reached in the exercise stress test to VO₂max reached during cold stress. Both stressors resulted in a similar VO₂max

in B6 controls but cold stress induced a higher VO_{2max} in ANT1 mice (Figure 2B). This also indicates a peripheral limitation in ANT1 mice. This is further supported by venous blood gas analysis performed of mice at rest or immediately after an exercise stress test. While there is no difference in the venous pO_2 between control and ANT1 mice at rest, ANT1 mice showed a significantly higher venous pO_2 after exercise (Figure 2C). This indicates that ANT1 mice have normal availability of oxygen to the muscle but insufficient oxygen extraction by the mitochondria. This is in line with no alterations in blood hemoglobin levels in ANT1 mice compared to B6 controls (Figure 2D). Lastly, we measured muscle pO_2 directly in the gastrocnemius muscle of anesthetized mice. At baseline, muscle pO_2 was similar between B6 control and ANT1 mice (Figure 2E).

However, after stimulation of the sciatic nerve, muscle pO_2 in ANT1 mice was significantly higher than in B6 controls (Figure 2F). Quantifying the decrease in muscle pO_2 upon stimulation revealed a significantly lower average and maximal rate of oxygen utilization in ANT1 mice (Figure 2G). This demonstrates that muscle oxygen consumption upon contraction is reduced in ANT1 mice.

In summary, using multiple lines of evidence, we demonstrated that skeletal muscle oxygen consumption limits the VO_2 in ANT1 mice.

3.3. NAD$^+$ availability stalls TCA cycle and limits skeletal muscle respiration in ANT1 mice upon exercise

To assess oxygen consumption in skeletal muscle directly, we performed high-resolution respirometry of the soleus muscle dissected from non-exercised (resting) mice. Surprisingly, we found no reduction in the OxPhos capacity (coupled respiration with excess complex I (CI) and complex II (CII) substrates, Figure 3A) and even an increase in the ETS capacity (uncoupled respiration, Figure 3B) in the ANT1 mice compared to B6 control when respiration rate was normalized to tissue mass (Table S1a). This is due to the >two-fold increase in mitochondrial mass of ANT1 mice compared to B6 controls (See Table S1b, ROS production upon AA as a surrogate marker for mitochondrial mass). Thus, while mitochondrial respiration per mitochondrion is lower in ANT1 mice [22], whole muscle mitochondrial respiratory capacities appear not to limit endogenous respiration (defined here as physiological respiration using endogenous substrates). We found a strongly increased ROS production in skeletal muscle of ANT1 mice compared to B6 control (Figure 3C, Table S1b). Thus, we hypothesized that excessive ROS production upon exercise might impair iron-sulfur clusters of the electron transport system, resulting in lower skeletal muscle respiration and the decreasing VO_2 upon exercise. To check this hypothesis, we ran mice until exhaustion, sacrificed them immediately afterwards and performed respirometry on soleus muscle. However, we did not observe a significantly lowered muscle respiration in acutely exercised ANT1 mice compared to muscle from resting mice (Figure 3A,B). Surprisingly, we found a significantly lower ROS production in skeletal muscle of acutely exercised ANT1 mice, indicating ROS-mediated inactivation of ETS enzymes did not occur upon exercise.

Interestingly, ANT1 mice showed a significantly lowered ratio of CI-linked to CII-linked respirational capacities (Figure 3D). We performed NADH fluorescence lifetime imaging microscopy (FLIM) of skeletal muscle and revealed a significantly shorter NADH lifetime, corresponding to a more reduced NAD$^+$/NADH redox state and a lower CI-linked respiration in ANT1 mice compared to B6 controls (Figure 3E). Given our ANT1 mice but not B6 controls also harbor the complex I variant ND5 m.12352C > T (ND5^{S204F}), we created additional control mice, called ND5 mice from here on out, harboring the ND5 m.12352C > T (ND5^{S204F}) variant. However, ND5 mice do not display a reduced VO_{2max} or running time, VO_2 does not decrease during exercise

(Figure S2a) and the CI to CII respirational capacities are similar to B6 controls. Thus, we conclude that the ANT1 mutation and not the ND5 variant is responsible for the phenotype of the ANT1 mice.

If mitochondrial capacities do not limit endogenous respiration, we hypothesized a substrate limitation. To further explore this hypothesis, we performed global metabolomics of gastrocnemius muscle of resting and acutely exercised mice. In B6 control mice, pathway analysis revealed an upregulation of TCA cycle, malate-aspartate shuttle, urea cycle and ammonium recycling metabolites immediately post-exercise (Figure S3a). In ANT1 mice, TCA cycle metabolites, urea cycle and ammonia recycling were also upregulated post-exercise (Figure S3b), however the malate-aspartate shuttle and the glucose alanine cycle were downregulated (Figure 3G). Having a closer look at TCA cycle metabolites showed a significant upregulation of most metabolites upon exercise both in B6 controls and ANT1 mice. However, α-ketoglutarate is significantly downregulated upon exercise in ANT1 skeletal muscle. This could indicate a lower activity of the isocitrate dehydrogenase, the first step in the TCA cycle requiring NAD$^+$, which might be lacking due to the lower CI-linked respiration (see Figure 3D). This is in line with a downregulation of the malate-aspartate shuttle in ANT1 skeletal muscle (Figure 3G). To maintain cytosolic NAD$^+$ levels and the essential glycolytic flux in ANT1 skeletal muscle, lactate is formed (see Figure 1F) and the Cori cycle might be preferred over the glucose—alanine cycle (Figure 3G), which would preserve the reducing equivalents and thus not recover NAD$^+$. In summary, pathway analysis of global metabolomics suggest alterations in many pathways associated with the NAD/NADH redox balance. However, it is crucial to emphasize that these findings rely on an overrepresentation of significantly altered metabolites in these pathways and do not necessarily suggest increased or decreased metabolic fluxes.

To further assess the possibility of an NAD $+$ limitation, we performed quantification of nucleotide levels in the gastrocnemius muscle. This revealed significantly reduced NAD $+$ levels in ANT1 mice (Figure S3e) but no change in the NAD/NADH ratio (Figure S3d), suggesting a lower NAD/NADH pool size in ANT1 muscle. This was confirmed by significantly lower mitochondrial NAD(H) levels quantified in isolated mitochondria from ANT1 gastrocnemius muscle. Absolute NAD$^+$ levels were increased significantly in ANT1 mice after exercise compared to resting mice (Figure S3e), suggesting an increase in the NAD/NADH pool size upon exercise in ANT1 mice. This is in line with a reduction in NAM levels upon exercise in ANT1 mice (Figure S3f) indicating an increase in the NAD$^+$ salvage pathway upon exercise, possibly to counteract for a lack of NAD$^+$. In contrast, we found no changes to the nucleotide levels in B6 control mouse skeletal muscle upon exercise (Figs. S3d—f).

In addition, global metabolomics revealed an upregulation of methylhistidine metabolism in ANT1 mice upon exercise (Figure S3b), indicating an increased protein catabolism. Combined with a downregulated ammonium ion export via the glucose—alanine cycle (Figure S3b) this might result in ammonium accumulation in skeletal muscle of ANT1 mice upon exercise, which was shown to further impair mitochondrial respiration [27].

In summary, we showed that complex I respiration is reduced in skeletal muscle of ANT1 mice. This likely results in a lack of NAD$^+$ to maintain the essential glycolytic flux, TCA cycle flux and ammonia recycling during exercise.

3.4. Nicotinamide riboside (NR) alleviates exercise intolerance in ANT1 mice

If NAD$^+$ availability in skeletal muscle is the limiting factor in ANT1 mice during exercise, boosting NAD$^+$ levels should improve exercise capacity in ANT1 mice.
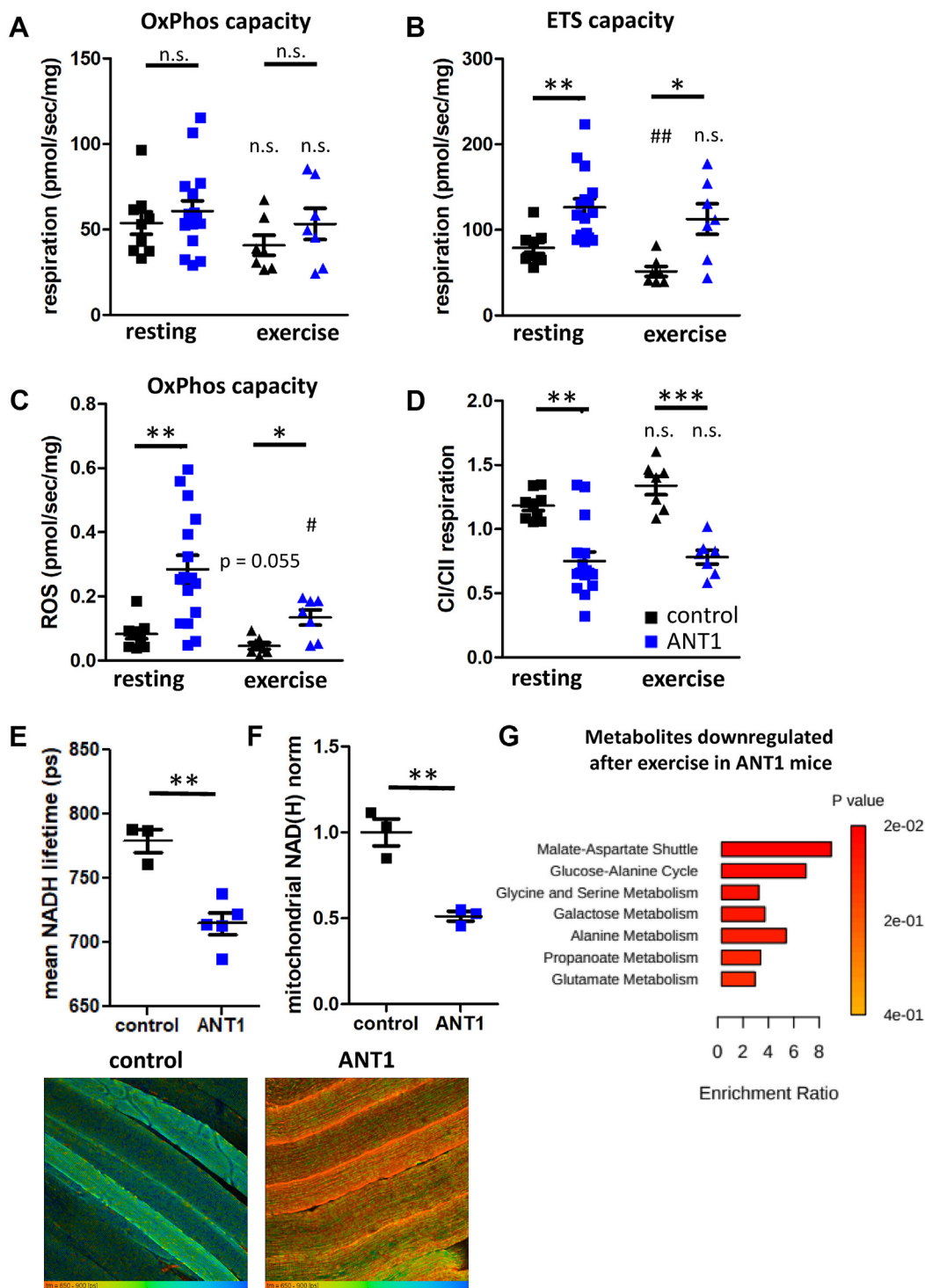
Figure 3: Reduced Complex I (CI)-linked respiration alters redox state and causes substrate limitation in ANT1 mice. **A/B/C)** Coupled (OxPhos capacity, (A)) and uncoupled (ETS capacity, (B)) respiration and ROS ($H_2O_2 + O_2^-$) production at OxPhos capacity (C) normalized to tissue mass in M. soleus of 6-month-old mice (n = 7−16) that were at rest or acutely exercised until exhaustion before being sacrificed. **D)** Ratio of CI to CII respiratory capacities in soleus of 6-month-old mice (n = 7−16) that were at rest or acutely exercised until exhaustion before being sacrificed. Significances between strains (*) and between resting and exercise (#) were calculated using Mann Whitney or unpaired t-test (*p < 0.05, **p < 0.01, ***p < 0.0001). **E)** Mean NAD(P)H lifetime measured by fluorescence lifetime imaging microscopy of NAD(P)H autofluorescence in M. gastrocnemius of 6-month-old mice (n = 3−5, 10 images each). NAD(P)H lifetime is false-color coded with red indicating a shorter NAD(P)H lifetime (more reduced NAD^+/NADH redox state) and blue indicating a longer NAD(P)H lifetime. **F)** NAD(H) levels in mitochondria isolated from gastrocnemius of 6-month-old mice (n = 3) **G)** Enrichment analysis of global metabolomics (downregulated metabolites, p < 0.05) in M. gastrocnemius of resting ANT1 mice compared to ANT1 mice exercised until exhaustion using Metascape. The enrichment ratio is indicated by the length of the bar and the p-value by color.
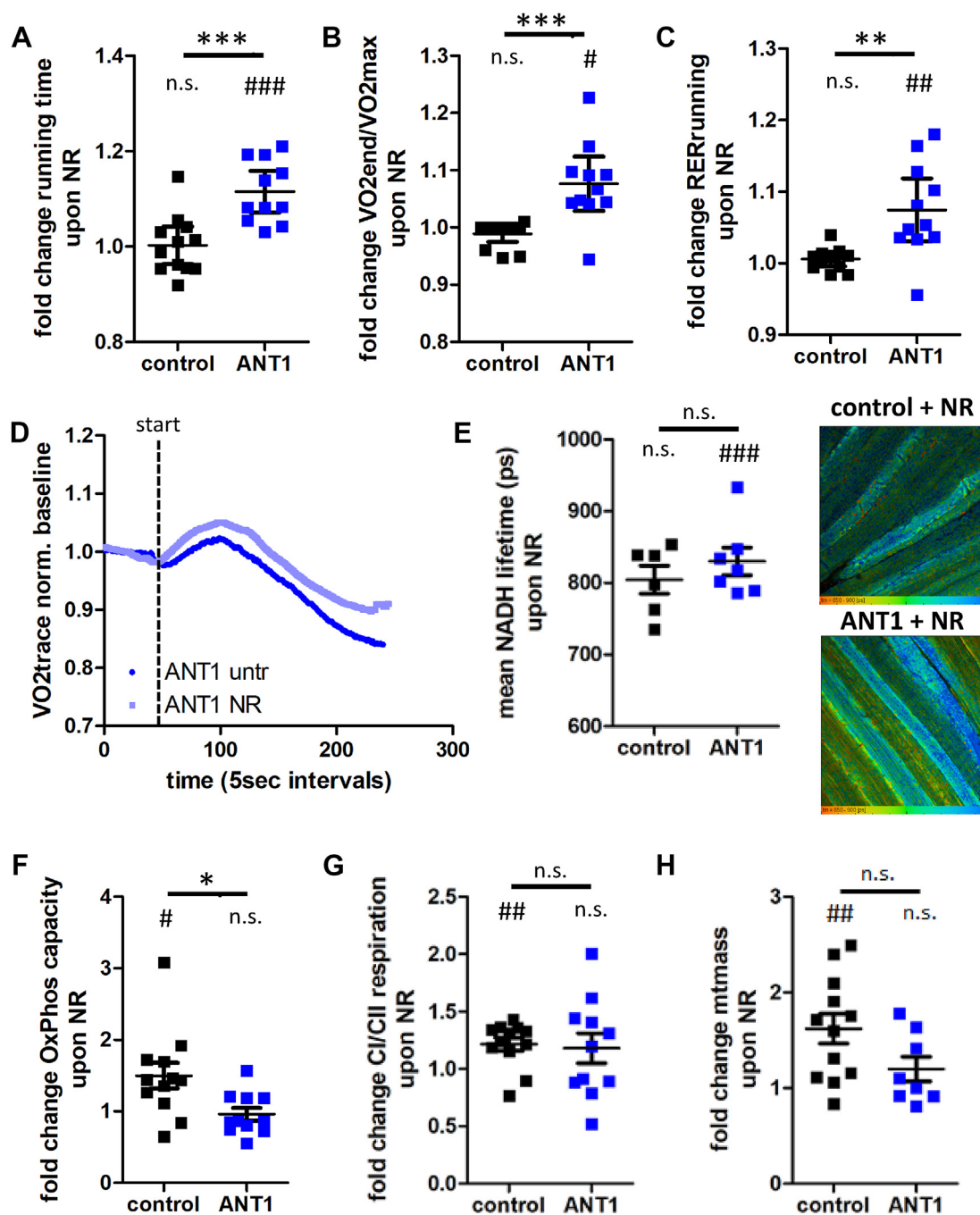
Figure 4: Nicotinamide riboside (NR) alleviates exercise intolerance in ANT1 mice. **A/B/C)** Fold change in running time (A), VO_2end/VO_2max (B) and RER (C) in an exercise stress test upon an 8-week treatment with NR in 6-month-old B6 control and ANT1 mice ($n = 11-12$). D) Average VO2 trace of an exercise stress test in 6-month-old ANT1 mice untreated (untr, dark blue) or treated with NR for 8 weeks (NR, light blue). E) Mean NAD(P)H lifetime in M. gastrocnemius of B6 control and ANT1 mice treated with NR ($n = 6-7$, 10 images each). NAD(P)H lifetime is false-color coded (same scale as for Figure 3e) with red indicating a shorter NAD(P)H lifetime and blue indicating a longer NAD(P)H lifetime. **F/G/H)** Fold change in M. soleus OxPhos capacity (F), CI/CII respirational capacity (G) and mitochondrial mass (H) upon an 8-week treatment with NR in 6-month-old B6 control and ANT1 mice ($n = 8-12$). Significances between strains (*) and between NR-treated and untreated (#) were calculated using Mann Whitney or unpaired t-test (*$p < 0.05$, **$p < 0.01$, ***$p < 0.0001$).

To test this hypothesis, we treated ANT1 and B6 control mice with 300 $mg/kg_{body\ weight}$ of NR orally with the food, starting at 4 months of age. NR treatment improved the running time of ANT1 mice but not B6 controls significantly (Figure 4A). In addition, NR increased the VO_2end/VO_2max (Figure 4B) in ANT1 mice, indicating a smaller drop in VO_2 during running (Figure 4D). While VO_2 at rest (Figure S4a) or VO_2max (Figure S4b) were not affected significantly.

NR treatment increased the VO_2 reserve capacity (Figure S4c) in both ANT1 and B6 control mice. Consistent with an increased glycolytic flux, NR treatment also increased both the RER at rest (Figure S4d) and during exercise (Figure 4C) in ANT1 mice. In the comprehensive lab animal monitoring system (CLAMS), control but not ANT1 mice showed a higher activity level (Figure S4e) and running wheel activity (Figure S4f).

NR significantly increased the reduced levels of NAD^+ content in the gastrocnemius muscle (Figure S3e) without changing the NAD/NADH ratio (Figure 4g and h). In contrast, neither NAD + levels nor NAD/NADH ratio were altered in the gastrocnemius of B6 control mice. Hence, oral NR treatment is effective for rescuing NAD^+ deficiency. We also performed NAD(P)H FLIM and found NR treatment increased NAD(P)H lifetime in the gastrocnemius muscle of ANT1 mice (Figure 4E).

To assess if the NR-effect is directly due to increased NAD^+ content or due to stimulated mitochondrial biogenesis and respiration, we performed respirometry on skeletal muscle. In B6 controls, we found NR increased OxPhos capacity (Figure 4F), CI/CII-linked respiration (Figure 4G) and mitochondrial mass (Figure 4H), consistent with stimulated mitochondrial biogenesis. However, the increased muscle respiration did not mediate an increased exercise capacity in B6 control mice consistent with their exercise capacity being limited by cardiovascular delivery of oxygen (see Figure 2). In contrast, in ANT1 mice, NR-treatment did not alter mitochondrial respiration (Figure 4F,G) or mitochondrial mass (Figure 4H) suggesting that the beneficial effect of NR on exercise ANT1 null capacity is due to an increased NAD^+ content.

We can conclude that NR treatment has a mildly positive effect on mice harboring the nuclear ANT1 mutation due to this mitochondrial defect resulting in reduced NAD^+ and NAD^+/NADH ratio. This suggests NAD + supplementation as a promising therapeutic intervention to alleviate exercise intolerance in ANT1-deficient patients and possibly other mitochondrial disorders.

4. DISCUSSION

Assessing the limiting factors of exercise capacity in ANT1-deficient mice, we gained three crucial insights how ANT1-deficiency alters exercise physiology and muscle metabolism. First, we discovered an unusual VO_2 kinetics during exercise, with VO_2 decreasing with increasing workload. We traced this effect to a substrate limitation in the skeletal muscle of NAD^+. Second, we found that ANT1-deficiency strongly shifts the mitochondrial respiration from CI-linked to CII-linked respiration in skeletal muscle, aggravating the NAD^+/NADH redox imbalance. Third, we observed that NAD + supplementation with NR can benefit the exercise intolerance in ANT1-deficient mice.

The VO_2 kinetics we observed in B6 control mice mirrors the VO_2 kinetics described for humans [28]. At moderate exercise levels, the VO_2 is proportional to the work load [29], thus increasing steadily with increasing running speed (see Figure 1A). At heavy exercise, VO_2 increases disproportionately to workload due to addition of the VO_2 slow component [30], resulting in the steeper rise in VO_2 towards the end of the exercise regime in B6 controls. The VO_2 kinetics at onset of exercise cannot be assessed in our system because mice are in a metabolic chamber. This causes a delay in detecting changes in the CO_2/O_2 ratio relative to activity which is not a concern in the breath-by-breath analysis common in human exercise studies.

In ANT1 mice we could demonstrate that VO_2 rises initially but then drops with increasing work load, a phenotype that becomes even more prominent with age. We found the VO_2 is limited by skeletal muscle oxygen consumption in ANT1 mice. This is consistent with pO_2 decreasing more slowly upon contraction in ANT1 skeletal muscle, indicating a lower endogenous mitochondrial respiration rate. In the ANT1 mice, we found similar respiratory capacities normalized to muscle weight as the B6 controls, and no indication of a reduced muscle mass, suggesting that the reduced exercise capacity was substrate limited. Based on global metabolomics after acute exercise,

respirometry, and rescue with NR we conclude that lack of NAD^+ might cause a stalling of the TCA cycle and reducing endogenous respiration. In line with this hypothesis, mice deficient for NAD^+ due to deletion of Nampt in skeletal muscle show a lower exercise capacity and mitochondrial respiration [31]. It would be interesting to see if the Nampt-deficient mice show a similar VO_2 kinetics during exercise as ANT1 mice.

While NR reduced the effect of decreasing VO_2 during exercise in ANT1 mice, it did not abolish it. Hence NAD + limitation is not the only factor limiting ANT1+ muscle performance. ANT1 mice also have an altered glucose homeostasis and we could show that they heavily rely on carbohydrates during exercise, resulting in hypoglycemia, which can cause fatigue [32]. Still, pyruvate levels were increased in skeletal muscle of ANT1 mice after exercise, contra-indicating a lack of glucose impairing respiration. Although we found no reduced respiration and even decreased ROS levels after an acute bout of exercise in ANT1 mice, we cannot exclude a temporary inhibition of iron sulfur clusters by ROS [33] or ammonium ions [27]. Tools to assess metabolic flux with a higher temporal resolution would be needed to fully elucidate the skeletal muscle metabolism of ANT1 mice during exercise.

Interestingly, we could demonstrate a shift from CI to CII respiration in skeletal muscle of ANT1 mice, resulting in a more reduced redox ratio. A lack of ATP/ADP exchange would be expected to result in a lower coupled respiration and a higher proton-motive force. One hypothesis for the switch from CI to CII respiration could be that CII does not pump protons, which might favor electrons entering the ETS via CII instead of CI. However, this would not explain why CI capacity is proportionately reduced compared to CII capacity in skeletal muscle of ANT1 mice. A previous study showed an upregulation of all mitochondrial gene expression in skeletal muscle of ANT1 mice, but the data reveal a tendency for a stronger upregulation of CII transcripts compared to CI transcripts [10]. Lastly, the higher ROS levels in ANT1 could partially inactivate iron-sulfur clusters of CI. The lower CI to CII respiration results in a more reduced NAD^+/NADH redox ratio, which contributes to the lack of NAD^+. Also, the NAD^+/NADH ratio is known to mediate mitochondria-nuclear signaling for example by affecting histone modifications, which could further contribute to the pathological phenotype of ANT1 mice.

We observed that NR improved the exercise capacity in ANT1 mice but not B6 control mice. These results are consistent with the differential effects of NR on rodent exercise capacity with some studies reporting beneficial effects [34,35], no effects [19,36], or negative effects [37]. It has been suggested that boosting NAD^+ is more effective in aged individuals than younger ones [35,38] due to the decreasing levels of NAD^+ and NAD salvage pathway expression with age (reviewed in [13]). Given NR did not increase NAD^+ levels in B6 mice, this could explain why we observed no positive effects in this strain. In contrast, ANT1 mice show slightly reduced NAD^+ levels and a reduced expression of Nampt, possibly due to increased inflammation and oxidative stress [39].

ANT1 null mutations cause myopathy and cardiomyopathy in humans [40]. It has been shown that redox imbalance and Nampt deficiency in the heart can contribute to heart failure [41,42], suggesting a possible role of NAD^+ deficiency in mediating cardiac remodeling in ANT1 null patients. In contrast, ANT1 missense mutations mostly affect the extraocular muscles (EOM) in humans. Interestingly, lactate dehydrogenase expression levels are low in human EOM compared to other skeletal muscles [43]. This indicates that EOM have a limited capacity to recover NAD^+ independent of CI-linked mitochondrial respiration and points to a possible lack of NAD^+ in the context of human ANT1-mediated progressive external ophthalmoplegia. Indeed, a recent study

in patients with progressive external ophthalmoplegia could demonstrate an altered NAD^+ metabolome and an improved muscle strength after boosting NAD^+ levels using niacin [18]. They further describe an increased mitochondrial biogenesis and mitochondrial respiration upon 4-months of niacin [18]. In contrast, we did not observe an increased mitochondrial biogenesis but our results suggest that the positive effect of NR is likely directly due to increased NAD^+ availability enabling an increased glycolytic flux, as indicated by the elevated RER during running.

In summary, we demonstrate a beneficial effect of NR in mitochondrial myopathy and associated exercise intolerance in mice that is dependent on the underlying mitochondrial mutation and its effects on exercise physiology.

AUTHOR CONTRIBUTIONS

P.M.S. and D.C.W. conceptualized the project and designed research; P.M.S., J.H., A.B., C·P., T.J, W.T. and R.M. performed research; P.M.S. and J.H. analyzed data; P.M.S., J.B. and D.C.W. interpreted the data, P.M.S. and D.C.W. wrote the paper. All authors read, edited and approved the manuscript.

FUNDING

MATERIAL AVAILABILITY

This study did not generate new unique reagents or organisms.

DATA AND CODE AVAILABILITY

All data is included in the manuscript or supplementary file. Any additional information required to reanalyze the data reported in this paper in available from the lead contact upon request.

Global metabolomics will be deposited at a suitable repository and made publicly available as of the date of publication.

DATA AVAILABILITY

Data will be made available on request.

ACKNOWLEDGEMENTS

CONFLICT OF INTEREST

Dr. Wallace is on the scientific advisory board of Pano Therapeutics and is a scientific advisor for Medical Excellence Capital. The other authors declare no conflicts of interest.

APPENDIX A. SUPPLEMENTARY DATA

Supplementary data to this article can be found online at https://doi.org/10.1016/j.molmet.2022.101560.

REFERENCES

[1] Karch, J., Bround, M.J., Khalil, H., Sargent, M.A., Latchman, N., Terada, N., et al., 2019. Inhibition of mitochondrial permeability transition by deletion of the ANT family and CypD. Science Advances 5(8):eaaw4597.

[2] Hoshino, A., Wang, W.J., Wada, S., McDermott-Roe, C., Evans, C.S., Gosis, B., et al., 2019. The ADP/ATP translocase drives mitophagy independent of nucleotide exchange. Nature 575(7782):375—379.

[3] Bertholet, A.M., Chouchani, E.T., Kazak, L., Angelin, A., Fedorenko, A., Long, J.Z., et al., 2019. Human Nature 571(7766):515—520.

[4] Kokoszka, J.E., Waymire, K.G., Levy, S.E., Sligh, J.E., Cai, J., Jones, D.P., et al., 2004. The ADP/ATP translocator is not essential for the mitochondrial permeability transition pore. Nature 427(6973):461—465.

[5] Bakker, H.D., Scholte, H.R., Van den Bogert, C., Ruitenbeek, W., Jeneson, J.A., Wanders, R.J., et al., 1993. Deficiency of the adenine nucleotide translocator in muscle of a patient with myopathy and lactic acidosis: a new mitochondrial defect. Pediatric Research 33(4 Pt 1):412—417.

[6] Palmieri, L., Alberio, S., Pisano, I., Lodi, T., Meznaric-Petrusa, M., Zidar, J., et al., 2005. Complete loss-of-function of the heart/muscle-specific adenine nucleotide translocator is associated with mitochondrial myopathy and cardiomyopathy. Human Molecular Genetics 14(20):3079—3088.

[7] Kawamata, H., Tiranti, V., Magrané, J., Chinopoulos, C., Manfredi, G., 2011. adPEO mutations in ANT1 impair ADP-ATP translocation in muscle mitochondria. Human Molecular Genetics 20(15):2964—2974.

[8] Graham, B.H., Waymire, K.G., Cottrell, B., Trounce, I.A., MacGregor, G.R., Wallace, D.C., 1997. A mouse model for mitochondrial myopathy and cardiomyopathy resulting from a deficiency in the heart/muscle isoform of the adenine nucleotide translocator. Nature Genetics 16(3):226—234.

[9] Yin, H., Stahl, J.S., Andrade, F.H., McMullen, C.A., Webb-Wood, S., Newman, N.J., et al., 2005. Eliminating the Ant1 isoform produces a mouse with CPEO pathology but normal ocular motility. Investigative Ophthalmology & Visual Science 46(12):4555—4562.

[10] Morrow, R.M., Picard, M., Derbeneva, O., Leipzig, J., McManus, M.J., Gouspillou, G., et al., 2017. Mitochondrial energy deficiency leads to hyperproliferation of skeletal muscle mitochondria and enhanced insulin sensitivity. Proceedings of the National Academy of Sciences of the United States of America 114(10):2705—2710.

[11] Sparks, L.M., Gemmink, A., Phielix, E., Bosma, M., Schaart, G., Moonen-Kornips, E., et al., 2016. ANT1-mediated fatty acid-induced uncoupling as a target for improving myocellular insulin sensitivity. Diabetologia 59(5):1030—1039.

[12] Imai, S., Guarente, L., 2014. NAD+ and sirtuins in aging and disease. Trends in Cell Biology 24(8):464—471.

[13] Verdin, E., 2015. NAD^+ in aging, metabolism, and neurodegeneration. Science 350(6265):1208—1213.

[14] Yoshino, J., Baur, J.A., Imai, S.I., 2018. NAD+ intermediates: the biology and therapeutic potential of NMN and NR. Cell Metabolism 27(3):513—528.

[15] Romani, M., Sorrentino, V., Oh, C.M., Li, H., de Lima, T.I., Zhang, H., et al., 2021. NAD+ boosting reduces age-associated amyloidosis and restores mitochondrial homeostasis in muscle. Cell Reports 34(3):108660.

[16] Remie, C.M.E., Roumans, K.H.M., Moonen, M.P.B., Connell, N.J., Havekes, B., Mevenkamp, J., et al., 2020. Nicotinamide riboside supplementation alters body composition and skeletal muscle acetylcarnitine concentrations in healthy obese humans. American Journal of Clinical Nutrition 112(2):413—426.

Brief Communication

[17] Yoshino, M., Yoshino, J., Kayser, B.D., Patti, G.J., Franczyk, M.P., Mills, K.F., et al., 2021. Nicotinamide mononucleotide increases muscle insulin sensitivity in prediabetic women. Science 372(6547):1224—1229.

[18] Pirinen, E., Auranen, M., Khan, N.A., Brilhante, V., Urho, N., Pessia, A., et al., 2020. Niacin cures systemic NAD+ deficiency and improves muscle performance in adult-onset mitochondrial myopathy. Cell Metabolism 31(6):1078—1090 e5.

[19] Cerutti, R., Pirinen, E., Lamperti, C., Marchet, S., Sauve, A.A., Li, W., et al., 2014. NAD(+)-dependent activation of Sirt1 corrects the phenotype in a mouse model of mitochondrial disease. Cell Metabolism 19(6):1042—1049.

[20] Khan, N.A., Auranen, M., Paetau, I., Pirinen, E., Euro, L., Forsström, S., et al., 2014. Effective treatment of mitochondrial myopathy by nicotinamide riboside, a vitamin B3. EMBO Molecular Medicine 6(6):721—731.

[21] Komlódi, T., Sobotka, O., Krumschnabel, G., Bezuidenhout, N., Hiller, E., Doerrier, C., et al., 2018. Comparison of mitochondrial incubation media for measurement of respiration and hydrogen peroxide production. Methods in Molecular Biology 1782:137—155.

[22] Schaefer, P.M., Rathi, K., Butic, A., Tan, W., Mitchell, K., Wallace, D.C., 2022. Mitochondrial mutations alter endurance exercise response and determinants in mice. Proceedings of the National Academy of Sciences of the United States of America 119(18) e2200549119.

[23] Zhou, Y., Zhou, B., Pache, L., Chang, M., Khodabakhshi, A.H., Tanaseichuk, O., et al., 2019. Metascape provides a biologist-oriented resource for the analysis of systems-level datasets. Nature Communications 10(1):1523.

[24] Lanfear, D.E., Gibbs, J.J., Li, J., She, R., Petucci, C., Culver, J.A., et al., 2017. Targeted metabolomic profiling of plasma and survival in heart failure patients. JACC Heart Fail 5(11):823—832.

[25] Horton, J.L., Davidson, M.T., Kurishima, C., Vega, R.B., Powers, J.C., Matsuura, T.R., et al., 2019. The failing heart utilizes 3-hydroxybutyrate as a metabolic stress defense. JCI Insight 4(4).

[26] Edvardsen, E., Hem, E., Anderssen, S.A., 2014. End criteria for reaching maximal oxygen uptake must be strict and adjusted to sex and age: a cross-sectional study. PLoS One 9(1):e85276.

[27] Davuluri, G., Allawy, A., Thapaliya, S., Rennison, J.H., Singh, D., Kumar, A., et al., 2016. Hyperammonaemia-induced skeletal muscle mitochondrial dysfunction results in cataplerosis and oxidative stress. Journal of Physiology 594(24):7341—7360.

[28] Xu, F., Rhodes, E.C., 1999. Oxygen uptake kinetics during exercise. Sports Medicine 27(5):313—327.

[29] Barstow, T.J., Casaburi, R., Wasserman, K., 1993. O2 uptake kinetics and the O2 deficit as related to exercise intensity and blood lactate. Journal of Applied Physiology 75(2):755—762.

[30] Gaesser, G.A., Poole, D.C., 1996. The slow component of oxygen uptake kinetics in humans. Exercise and Sport Sciences Reviews 24:35—71.

[31] Frederick, D.W., Loro, E., Liu, L., Davila, A., Chellappa, K., Silverman, I.M., et al., 2016. Loss of NAD homeostasis leads to progressive and reversible degeneration of skeletal muscle. Cell Metabolism 24(2):269—282.

[32] Brun, J.F., Dumortier, M., Fedou, C., Mercier, J., 2001. Exercise hypoglycemia in nondiabetic subjects. Diabetes & Metabolism 27(2 Pt 1):92—106.

[33] Flint, D.H., Tuminello, J.F., Emptage, M.H., 1993. The inactivation of Fe-S cluster containing hydro-lyases by superoxide. Journal of Biological Chemistry 268(30):22369—22376.

[34] Cantó, C., Houtkooper, R.H., Pirinen, E., Youn, D.Y., Oosterveer, M.H., Cen, Y., et al., 2012. The NAD(+) precursor nicotinamide riboside enhances oxidative metabolism and protects against high-fat diet-induced obesity. Cell Metabolism 15(6):838—847.

[35] Zhang, H., Ryu, D., Wu, Y., Gariani, K., Wang, X., Luan, P., et al., 2016. NAD+ repletion improves mitochondrial and stem cell function and enhances life span in mice. Science 352(6292):1436—1443.

[36] Crisol, B.M., Veiga, C.B., Braga, R.R., Lenhare, L., Baptista, I.L., Gaspar, R.C., et al., 2020. NAD+ precursor increases aerobic performance in mice. European Journal of Nutrition 59(6):2427—2437.

[37] Kourtzidis, I.A., Stoupas, A.T., Gioris, I.S., Veskoukis, A.S., Margaritelis, N.V., Tsantarliotou, M., et al., 2016. The NAD(+) precursor nicotinamide riboside decreases exercise performance in rats. Journal of the International Society of Sports Nutrition 13:32.

[38] Dolopikou, C.F., Kourtzidis, I.A., Margaritelis, N.V., Vrabas, I.S., Koidou, I., Kyparos, A., et al., 2020. Acute nicotinamide riboside supplementation improves redox homeostasis and exercise performance in old individuals: a double-blind cross-over study. European Journal of Nutrition 59(2):505—515.

[39] Krzysik-Walker, S.M., Hadley, J.A., Pesall, J.E., McFarland, D.C., Vasilatos-Younken, R., Ramachandran, R., 2011. Nampt/visfatin/PBEF affects expression of myogenic regulatory factors and is regulated by interleukin-6 in chicken skeletal muscle cells. Comparative Biochemistry and Physiology Part A: Molecular & Integrative Physiology 159(4):413—421.

[40] Echaniz-Laguna, A., Chassagne, M., Ceresuela, J., Rouvet, I., Padet, S., Acquaviva, C., et al., 2012. Complete loss of expression of the ANT1 gene causing cardiomyopathy and myopathy. Journal of Medical Genetics 49(2):146—150.

[41] Lee, C.F., Chavez, J.D., Garcia-Menendez, L., Choi, Y., Roe, N.D., Chiao, Y.A., et al., 2016. Normalization of NAD+ redox balance as a therapy for heart failure. Circulation 134(12):883—894.

[42] Byun, J., Oka, S.I., Imai, N., Huang, C.Y., Ralda, G., Zhai, P., et al., 2019. Both gain and loss of Nampt function promote pressure overload-induced heart failure. American Journal of Physiology - Heart and Circulatory Physiology 317(4):H711—H725.

[43] Fischer, M.D., Gorospe, J.R., Felder, E., Bogdanovich, S., Pedrosa-Domellöf, F., Ahima, R.S., et al., 2002. Expression profiling reveals metabolic and structural components of extraocular muscles. Physiological Genomics 9(2):71—84.